

CORROSION TESTING OF NICRAL(Y) COATING ALLOYS IN HIGH-TEMPERATURE AND SUPERCRITICAL WATER

Stephan Biljan¹, Xiao Huang¹, Yunfen Qian¹ and David Guzonas²

¹Carleton University, Ottawa, Ontario, Canada

²Atomic Energy of Canada Limited, Chalk River Laboratories, Ontario, Canada

Abstract

With the development of Generation IV (Gen IV) nuclear power reactors, materials capable of operating in high-temperature and supercritical water environment are essential. This study focuses on the corrosion behavior of five alloys with compositions of Ni20Cr, Ni5Al, Ni50Cr, Ni20Cr5Al and Ni20Cr10AlY above and below the critical point of water. Corrosion tests were conducted at three different pressures, while the temperature was maintained at 460°C, in order to examine the effects of water density on the corrosion. From the preliminary test results, it was found that the binary alloys Ni20Cr and Ni50Cr showed weight loss above the critical point (23.7 MPa and 460°C). The higher Cr content alloy Ni50Cr suffered more weight loss than Ni20Cr under the same conditions. Accelerated weight gain was observed above the critical point for the binary alloy Ni5Al. The combination of Cr, Al and Y in Ni20Cr10AlY provides stable scale formation under all testing conditions employed in this study.

1. Introduction

Concerns with greenhouse gas emissions and the uncertainty of a long-term supply of fossil fuels have resulted in renewed interest in nuclear energy as an essential part of the energy mix for the future. A joint international effort has been devoted to develop Generation-IV reactor technologies that will have enhanced efficiencies and be sustainable for the future. They must also be competitive with other technologies, operate more safely and reliably and be more proliferation resistant and physically robust [1]. One of the six reactor designs being considered in the Gen-IV program is the Supercritical Water-Cooled Reactor (SCWR). This concept calls for the use of single-phase SCW as the coolant, which will lead to plant simplification and high thermodynamic efficiency [as high as 49% vs. 33% for current reactors]. Reactor operating conditions can vary from 280 to 620°C at a typical pressure of 25 MPa [2],[3].

Water is in a supercritical state at a temperature above 374°C and a pressure above 22.05 MPa. A supercritical fluid has properties that are intermediate between a gas and a liquid and is often considered comparable to a dense gas. The unique, extensively hydrogen-bonded structure of water leads to significant changes in the properties of water as it passes through the critical point. The density and ionic dissociation of water decrease significantly at or above the point of transition from the subcritical to the supercritical state. The abrupt shift in physical properties is expected to influence the corrosion behavior of materials, and the point of transition in physical properties, rather than the point of transition to the supercritical state, might be expected to better delineate the corrosion behavior. Water changes with temperature and pressure from a high density, high polarity solvent to a low density, low polarity solvent [5]. In addition to changes in

water density, the solubility of ions in water varies with temperature and pressure. At 25 MPa the dissociation of water, $\text{H}_2\text{O} \rightarrow \text{H}^+ + \text{OH}^-$, peaks at a temperature around 300°C, with an ionic product concentration that is about 3 orders of magnitude greater than that at room temperature. As water transitions to supercritical, there is a pronounced reduction in ion product, being about 13 orders of magnitude lower at 500°C than at 300°C. As a result, the solubility of many metal oxides decreases above the critical point [4]. Most metal oxides show increased solubility in either acidic or alkaline solutions, so an increase in the ion character of water typically leads to an increase in corrosion [5].

The solubility of oxygen is another consideration. Increasing the oxygen concentration increases the initial oxidizing power of the solution and subsequently the corrosion rate [6]. However, increased oxygen concentration also has been shown to be beneficial by retarding crack growth rates of 316L stainless steel due to crack tip blunting when tested in SCW between 400°C to 500°C [7].

The identification of appropriate materials to contain the SCW fluid will be one of the major challenges for the development of the SCWR. In the various conceptual designs of the SCWR, water goes through the critical point twice (in the reactor core and in the turbine) as it circulates around the heat transport loop. Well above the critical temperature, the density of SCW is sufficiently low that the corrosion is expected to be similar to that found in high temperature steam. Below the critical temperature, materials will exhibit corrosion rates similar to those observed in high density hot liquid water, but at temperatures above those of currently operating reactors. These unique changes in the properties of water above and below the critical point complicate the choice of materials, which must therefore be selected such that they can withstand the type of corrosion expected in the particular environment to which they are exposed [8].

Ferritic-martensitic (F/M) steels (Fe-Cr based), austenitic steels and Ni-based alloys are some of the candidate materials being considered for SCWR applications. The corrosion performance of T91 (Fe-9Cr-Mo), T92 (Fe-9Cr-W), T122 (Fe-12Cr) and Ni-based alloys 625, 690, Incoloy 800H have been tested at 25 MPa and temperatures ranging from 370°C to 600°C in de-ionized water with less than 10 ppb of dissolved oxygen (DO) [9]. At lower supercritical temperatures or in subcritical water, the corrosion rate of the F/M steels after 200 hrs was low and not substantially different from the nickel alloys. As temperature increased, the corrosion resistance of the F/M steels became inferior to that of the nickel-based alloys. Further tests on T91 [10] showed that in sub-critical water (370°C, 25 MPa) corrosion was by ionic dissolution and a much thinner protective oxide formed. F/M alloys also had higher corrosion rates than austenitic steels [10]. When T91 samples were exposed to supercritical water at 500°C with two different dissolved oxygen (DO) concentrations, 0.025 ppm and 2 ppm [11], the oxide layer formed on T91 at low oxygen concentration was stable and more protective than the oxide formed at the high oxygen concentration. At the low DO concentration, a duplex oxide structure was formed consisting of an outer layer of magnetite (Fe_3O_4) and an inner layer of chromite (FeCr_2O_4). At the high DO level, a hematite (Fe_2O_3) surface layer formed and the underlying layers were more porous and less adherent to the substrate.

Austenitic stainless steels, such as 304, 316 and 800H [12], showed lower corrosion rates in supercritical water; however, the rate increased substantially in subcritical water [13]. It was also

found that the oxide formed on austenitic stainless steels has the tendency to spall [14]. Nickel-base alloys in generally are relatively immune to corrosion in SCW but corrosion can be high in subcritical water [6],[14]. Additionally, nickel-base super-alloys exhibit greater susceptibility to localized pitting and inter-granular stress corrosion cracking than ferritic-martensitic stainless steels [15].

Based on the above brief summary, it is seen that the corrosion in water is sensitive to both testing conditions and alloy composition. Most of the alloys tested suffer from one or more modes of corrosion under different conditions (temperature, pressure, water chemistry, and stress). For alloys that rely on the formation of protective chromia to provide corrosion resistance, the formation of soluble hexavalent chromium (CrO_4^{2-} (chromate), HCrO_4^- or H_2CrO_4) can render the oxide layer non-protective [5],[17],[18]. The addition of Al is considered in this study since Al_2O_3 has shown superior corrosion resistance to most of the aqueous conditions, whether supercritical [19] or steam [20].

This study aims at investigating the corrosion behavior of several potential coating compositions in high-temperature and supercritical water. Specifically, coating compositions of Ni-Cr, Ni-Al, Ni-Cr-Al and Ni-Cr-Al-Y are being examined in this study.

Extensive corrosion and oxidation coating development in gas and steam turbines resulted in the widespread use of MCrAlY, M = Ni, NiCo, CoNi, or Fe based coating compositions [21],[22],[23],[24]. (Co cannot be used in nuclear reactor applications because it can be neutron activated to ^{60}Co [25]. It was therefore excluded from this study.) MCrAlY coatings form dense adherent alumina and/or chromia films (via the oxidation of aluminum and/or chromium) to provide corrosion resistance. The basic microstructure of MCrAlY coatings consists of β -NiAl aluminide embedded in more ductile γ -Ni (Fe,Cr,Co) solid solution.

The test conditions were selected to provide varying water densities while maintaining a constant temperature of 460°C.

2. Materials and Experimental Methods

To test the corrosion resistance of Ni-based coating compositions in high-temperature and supercritical water, five 12.7 mm dia. rods with compositions given in Table 1 were manufactured by vacuum casting and HIPing (Sophisticated Alloys, USA). The reason for studying bulk materials instead of coatings was based on the need to identify first if Al addition to Ni-Cr alloy system would be beneficial for supercritical water reactor application. Additionally, coating performance largely depends upon both alloy composition and microstructure (influenced by coating processes). As such, bulk materials with varying compositions were studied first in this research. Each rod was cut to a sample size of 5 mm in thickness using a lathe and abrasive saw (Buehler Isomet 1000 precision saw). One side of sample was then ground using a belt sander and polished to 600 grit. The samples were cleaned with alkaline solution in a 2520 Branson Ultrasonic cleaner. Before testing, the samples were cleaned with methanol and weighed. The samples were then placed, polished faces up, on a ceramic disc in the autoclave in order to prevent contact with the autoclave wall.

Three different tests were conducted in autoclaves supplied by Parr Instrument (Parr 4650 combined with a Parr 4838 reactor controller). A vacuum was first created in the system to remove oxygen. A set amount of water, calculated based on temperature, volume of the autoclave and target pressure, was inserted into the vessel. Three different pressures were used in this study to examine the impact of water density on the corrosion behaviour of different alloy compositions. The DO concentration in the water was controlled by distillation and nitrogen gas bubbling, and the DO concentration at the start of the test was measured before each test run. The autoclave was then heated to 460°C. Details on test temperature, pressure, duration, and DO concentration are summarized in Table 2. Due to the leakage of the autoclaves, the pressure at the end of the test was below that at the start as reported in Table 2.

Upon termination of the tests, samples were weighed and the weights before and after the tests are given in Table 3. A precision scale (Mettler Toledo AG285 with a minimum tolerance of +/- 0.005 mg) was used to weigh samples before and after testing. Microstructure analysis was carried out followed by Scanning Electron Microscope (SEM) analysis using a Vega II XMU. EDS analysis of the surface compositions was also carried out using an Oxford EDEX system.

Table 1 Sample chemical compositions (wt. %).

	Ni	Cr	Al	Y
Sample 1 - Ni20Cr	Bal.	20	-	-
Sample 2 - Ni5Al	Bal.	-	5	-
Sample 3 - Ni50Cr	Bal.	50	-	-
Sample 4 - Ni20Cr5Al	Bal.	20	5	
Sample 5 - Ni20Cr10AlY	Bal.	20	10	1

Table 2 Test conditions.

	Temperature (°C)	Pressure (start) (MPa)	Pressure (end) (MPa)	Density (g/cm ³)	Time (hr)	DO level (ppm)
Test 1	460	11.7	5.5	40.2	166	2
Test 2	460	17.2	13.1	64.4	158	1
Test 3	460	23.8	19.7	101.1	167	2

3. Results

3.1 Visual observation

Upon removing the samples from the autoclaves after testing, their surface appearances were recorded, as shown in Figure 1 and Table 3. All samples displayed unique surface colorations,

indicative of different surface film thicknesses, compositions and densities. In general, sample 2 (Ni5Al) showed the darkest surface film while sample 5 (Ni20Cr10AlY) had the lightest colored surface film under all test conditions. For other samples, the surface films varied with composition and test conditions. For example, sample 1 (Ni20Cr) showed a lighter-colored surface film at an intermediate test pressure (test 2 of 17.2 MPa) while sample 3 (Ni50Cr) showed different surface film colors under all three test conditions. Sample 4 (Ni20Cr5Al), with 5% Al added to sample 1 (Ni20Cr), displayed a lighter-colored surface film than sample 1 under all conditions.

The visual observation suggests that additions of both Al and Cr to Ni in general reduce the surface film formation, a synergistic effect of Cr and Al seen in other corrosion and oxidation resistant alloys [26]. Additionally, increasing the pressure from 11.7 to 24 MPa changed the surface film appearances for sample 1 (Ni20Cr), sample 3 (Ni50Cr) and sample 4 (Ni20Cr5Al), although no quantitative trend can be observed through visual inspection.



(b)

Figure 1 Sample surface appearances after testing.

3.2 Weight change

Table 3 summarizes the sample weights measured before and after the tests. The individual sample weight change, the weight difference before and after each test normalized by total sample surface area, was also calculated and is displayed in bar charts shown in Figure 2. When comparing the weight changes of samples, weight gain normally indicates surface film formation while weight loss represents metal dissolution or surface film dissolution and spalling.

Table 3 Summary weight changes and sample surface appearances after tests.

Sample Number (Test No.)	Weight before testing (g)	Weight after testing (g)	Weight change (mg)	Surface appearance after testing
1 (1) - Ni20Cr	5.2086	5.2087	0.1	Black
2 (1) - Ni5Al	5.0804	5.0806	0.2	Black
3 (1) - Ni50Cr	4.6842	4.6843	0.1	Blue

4 (1) - Ni20Cr5Al	4.3367	4.3367	0	Gold
5 (1) - Ni20Cr10AlY	4.5638	4.5640	0.2	Light Gold
1 (2) - Ni20Cr	5.2697	5.2700	0.3	Grey
2 (2) - Ni5Al	5.0283	5.0286	0.3	Black
3 (2) - Ni50Cr	4.7208	4.7209	0.1	Gold
4 (2) - Ni20Cr5Al	4.7806	4.7805	-0.1	Blue
5 (2) - Ni20Cr10AlY	4.6081	4.6084	0.3	Gold
1 (3) - Ni20Cr	5.4158	5.4158	0	Black
2 (3) - Ni5Al	5.1128	5.1133	0.5	Black
3 (3) - Ni50Cr	4.9135	4.9134	-0.1	Purple
4 (3) - Ni20Cr5Al	4.2712	4.2711	-0.1	Gold
5 (3) - Ni20Cr10AlY	4.8157	4.8159	0.2	Gold

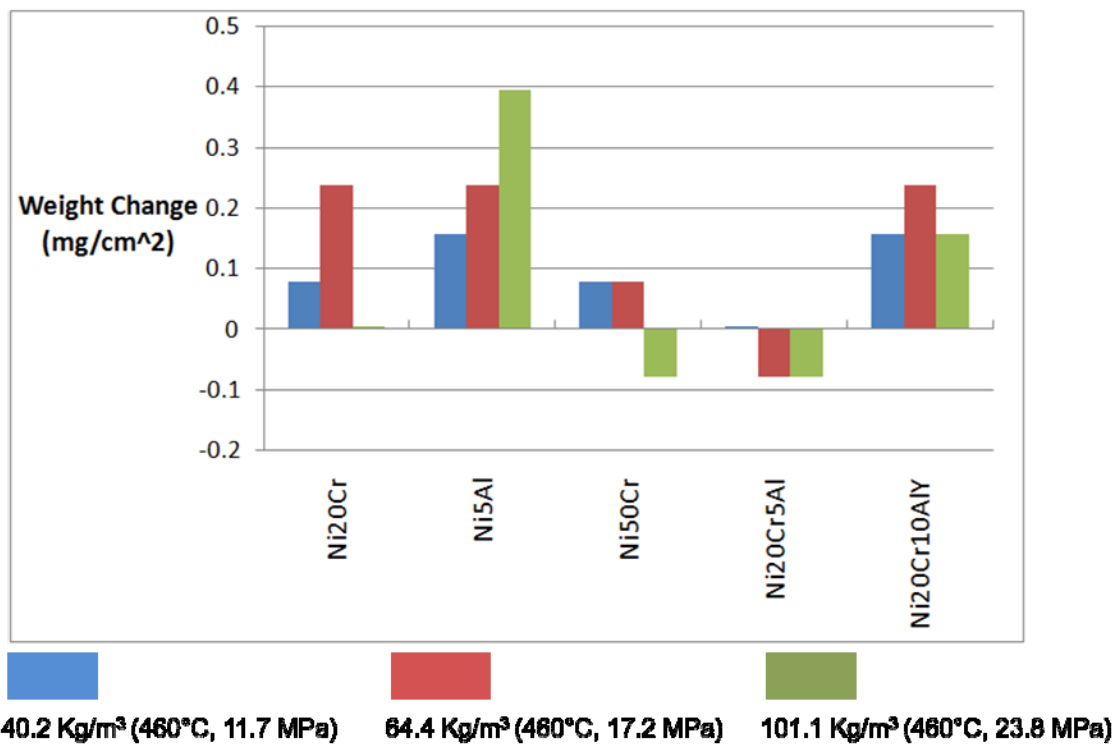


Figure 2 Weight changes for five coatings samples at three different water densities.

All samples showed weight gain after test 1 (at 460°C and 11.7MPa) with the exception of sample 4 (Ni20Cr5Al) which did not suffer any weight change. Samples 2 (Ni5Al) and 5 (Ni20Cr10AlY) had the most weight gains among all samples tested, suggesting oxide formation during the test. After test 2 (at 460°C and 17.2 MP) all samples except sample 4 (Ni20Cr5Al)

showed weight gain. Sample 1 (Ni20Cr), sample 2 (Ni5Al) and sample 5 (Ni20Cr10AlY) had similar values of weight gain and these values were greater than those after test 1. Sample 3 showed a similar weight change after test 1 and test 2. After being tested in supercritical water (460°C and 23.8MPa) the corrosion behavior changed more significantly. Samples 2 (Ni5Al) and 5 (Ni20Cr10AlY) showed weight gain, while samples 3 (Ni50Cr) and 4 (Ni20Cr5Al) exhibited weight loss. Sample 1 (Ni20Cr) had no net weight change.

Samples 1 (Ni20Cr) and sample 3 (Ni50Cr) showed similar trends in terms of weight changes vs. testing pressure. At 11.7 and 17.2 MPa, both samples show weight gain as a result of scale formation, although sample 3 with higher Cr content showed less weight gain at 17.2MPa than sample 1 with lower Cr. This suggests that higher Cr content may be beneficial under subcritical conditions. When the pressure was increased to 23.8 MPa (into the supercritical region), sample 1 showed no weight change although film formation was clearly seen in Figure 1. This suggests the possible presence of competing processes of surface film formation and dissolution. With increased Cr content in sample 3 (Ni50Cr), the dissolution process is further increased, causing weight loss to be observed in Figure 2, probably due to the formation of soluble hexavalent chromium [5],[18]. While previous studies have shown increased corrosion rate with pressure [5], [27], which is the case for sample 1 tested at 11.7 and 17.2 MPa, it is believed that there also exists a transition point where film formation shifts to film or metal dissolution with the increase in water density (from 40 to 64.4 g/cm³).

Sample 2, with Ni5Al, showed weight gain under all test conditions. NiO or/and Al₂O₃ are believed to have formed based on the observation of oxygen peak on the EDS spectrum; this led to the observed weight gain. Increasing the test pressure from 11.7 to 17.2 MPa gradually increased the weight gain and at 23.8 MPa, a drastic increase in weight gain was found. This suggests that the oxide(s) formed on Ni5Al was less protective allowing further oxidation to continue.

Sample 4, with Ni20Cr5Al, showed no weight change (test 1) or weight loss (tests 2 and 3) under various test conditions. Although no weight change (within the limit of the measuring device) was detected after test 1 (11.7MPa), the sample did show a change in surface appearances (Figure 1a). With the increase in pressure (test 2 and test 3), weight losses were observed for this sample, suggesting increased metal or oxide dissolution. Detailed surface and cross sectional microstructure analysis is being carried out using focused ion beam (FIB) sample milling and transmission electron microscopy (TEM) to examine the nature of the surface films formed at various pressures.

Sample 5 (Ni20Cr10AlY) showed consistent weight gain at all pressures, although a slightly higher weight gain was measured under sub-critical condition (17.2 MPa). This observation indicates that the oxidation behavior of this composition does not change much with test pressure and is in consistency with the visual inspection of sample 5 shown in Figure 1.

3.3 Scanning Electron Microscopy

The surface morphology of each sample was observed using SEM. Selected areas on the surface

were analyzed using EDS. From the observation of surface morphologies of the five samples tested at 460°C and 11.7 MPa, shown in Figure 3 (low magnification on the left and higher magnification on the right), the polishing lines can still be clearly seen. All samples revealed numerous surface irregularities, with sample 4 (Ni₂₀Cr₅Al) displaying the most surface irregularities/depressions than the others.

Corrosion products were only found on the surface of sample 5. It displayed unique surface features, including an etched grain structure and the formation of phases along the grain boundary region. SEM/EDS analysis was not able to identify the nature of these phases and further analysis is underway. As oxides form preferentially on grain boundary regions in NiCrAlY alloys upon exposure to an oxidizing environment [28], it is believed that these observed surface particles may be oxides of Ni, Cr and Al. The formation of surface oxides also support the weight gain observed for sample 5 after exposure to 460°C at 11.7MPa (Figure 2).

Surface composition analyses were carried out using EDS. The surface compositions of all samples were similar to those of the base alloys with the exception of the presence of Si and O (Figure 4) on the surface. Si was detected on all sample surfaces and this was believed to be the result of silicon sealing compound contamination. The presence of O peaks in some EDS spectra suggested oxide formation. However, no semi-quantitative measurements of O could be made with EDS.

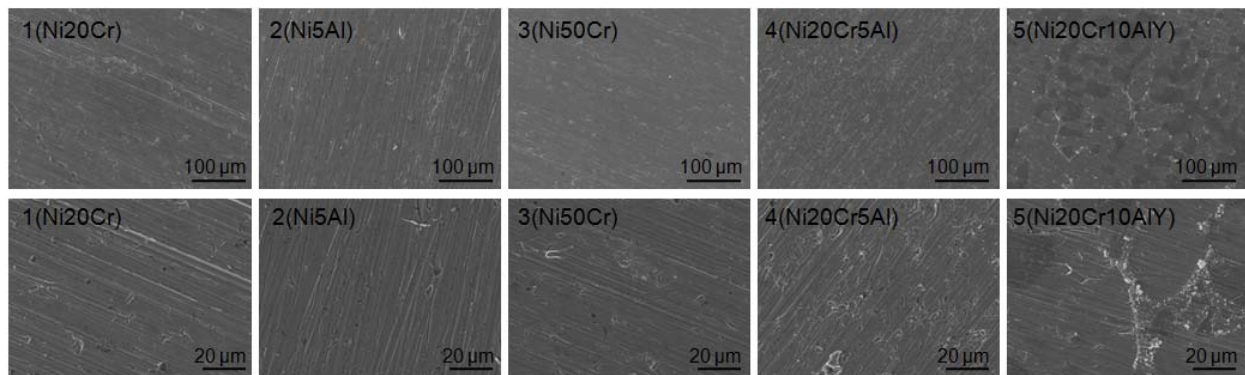


Figure 3 SEM images of samples after testing at 460°C and 11.7MPa (test 1).

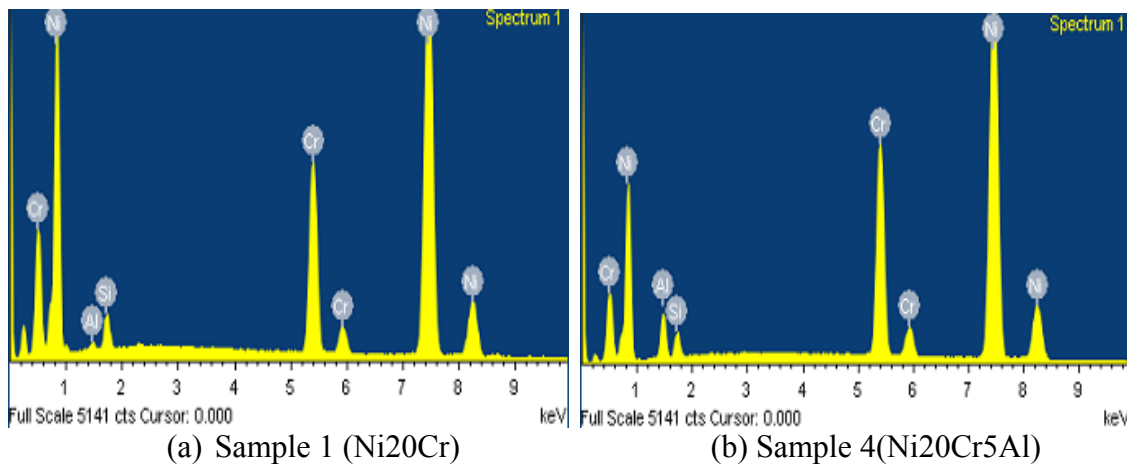
Table 4 EDS semi-quantitative surface analysis results for samples after test 1.

Wt%	Al	Cr	Si	Ni
Sample 1 (Ni ₂₀ Cr)	-	18.04	1.93	79.6
Sample 2 (Ni ₅ Al)	5.46	-	2.89	91.65
Sample 3 (Ni ₅₀ Cr)	-	47.79	8.02	44.2
Sample 4 (Ni ₂₀ Cr ₅ Al)	2.87	19.29	1.32	76.53
Sample 5 (Ni ₂₀ Cr ₁₀ AlY)	6.49	26.17	4.0	63.34

The surface morphologies of samples after test 2 at 460°C and 17.2 MPa are shown in Figure 5. Similar features to those seen in Figure 3 were observed after test 2; these included: polishing

lines, surface depressions and grain boundary phases on sample 5. After test 3 at 460°C and 23.8 MPa, sample 1 (Ni20Cr) and sample 2 (Ni5Al) showed particularly roughened surfaces after testing, while sample 3 (Ni50Cr) and sample 4 (Ni20Cr5Al) were similar to those tested under sub-critical conditions. Numerous white particles were observed on sample 3 but EDS could not identify the nature of these particles. Sample 5 (Ni20Cr10AlY) again revealed delineated grain structure and boundary phases.

The water pressure (density) had a notable effect on the corrosion behavior. Sample 1 had more surface depressions when tested under supercritical condition than under sub-critical conditions. This implies localized material removal and explains the reason for zero weight change after test 3 where both oxidation and material removal occurred simultaneously. The surface morphology on sample 2 changed little after test 1 and test 2 but became slightly more irregular after test 3. The weight gain observed under all test conditions suggests oxide formation though this was not observed directly in this study. Sample 3 did not show any noticeable surface morphology changes after all three tests, although the weight gain observed under 11.7 MPa and 17.2 MPa changed to weight loss under supercritical conditions. Furthermore, sample 4 exhibited surface depressions under all test conditions and was the only sample that did not show weight gain under any of the test conditions. Sample 5 showed similar weight gain and surface morphologies under all three test conditions, indicating that the corrosion behavior was not affected by water pressure/density.



(a) Sample 1 (Ni20Cr) (b) Sample 4(Ni20Cr5Al)
Figure 4 Example of EDS spectra taken from samples 1 (Ni20Cr) and 4 (Ni20Cr5Al) after testing at 460°C and 11.7MPa (test 1).

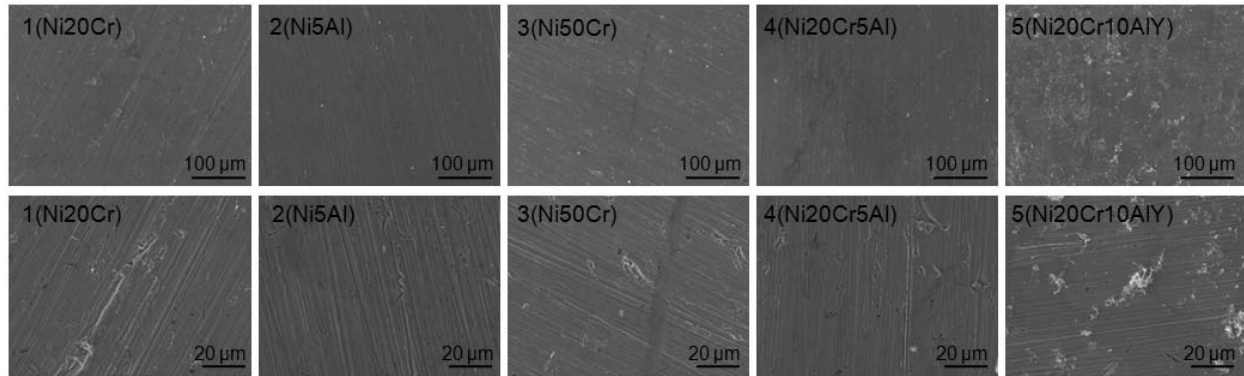


Figure 5 SEM images of samples after testing at 460°C and 17.2 MPa (test 2).

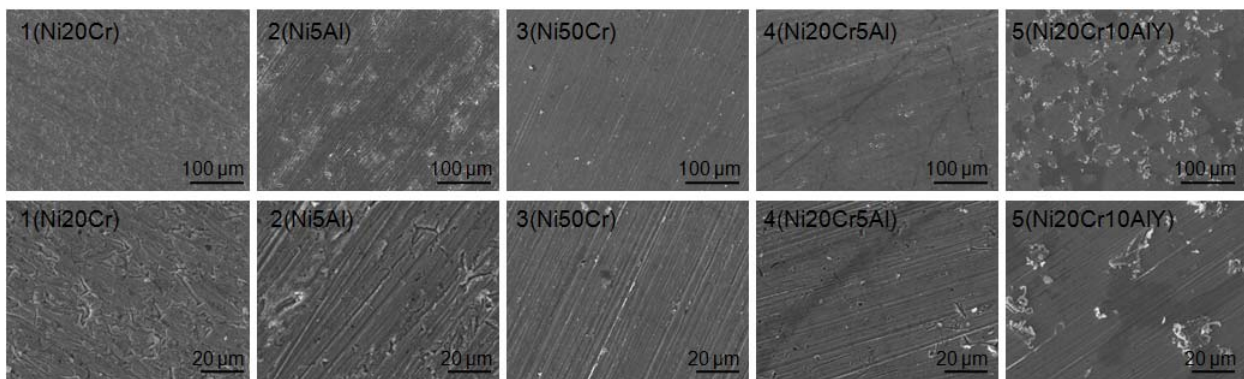


Figure 6 SEM images of samples after testing at 460°C and 23.8 MPa (test 3).

4. Conclusion and Future Work

The tests performed in this study enabled us to better understand the corrosion behavior of five alloys with respect to changes in water density at constant temperature. The following preliminary conclusions can be drawn based on this study:

- Binary NiCr alloys, Ni20Cr and Ni50Cr showed different corrosion modes in sub-critical and supercritical conditions. Higher Cr content suffers more weight loss in supercritical water due to the dissolution hexavalent Cr^{6+} .
- Binary NiAl alloy, Ni5Al, suffered from the most weight gain in supercritical water. Addition of Al may need to be combined with Cr (and Y) in order to provide protection against corrosion in high temperature and supercritical water.
- The NiCrAlY alloy exhibited the most stable scale formation under all testing conditions employed in this study.
- The increase in pressure caused different changes in corrosion modes among the samples tested. The increasing trend of corrosion with pressure was consistently observed in this study.

Future work on analyzing the nature of the surface film formed under different is being planned in collaboration CANMET under a RIEM program. Also, a SCW dynamic loop is being

constructed at Carleton University. Similar test will be carried out in the loop and the results will be compared to that obtained from static autoclaves.

5. Acknowledgement

The authors like to thank NSERC (National Science and Engineering Research Council) for providing collaborative research funding for this research. We also thank AECL for providing technical assistance with autoclaves.

6. List of references

- [1] U.S. DOE nuclear energy research advisory committee and Gen IV international forum (GIF), A technology roadmap for generation IV nuclear energy system, GIF 002-00, Dec. 2002.
- [2] J. Buongiorno, et al., "Supercritical water reactor: survey of materials experience and R&D needs to assess viability", INEEL/EXT-03-00693, Rev.1, Sept., 2003.
- [3] G. S. Was, et al. Corrosion and stress corrosion cracking in supercritical water, *Journal of Nuclear Materials*, Vol.371, 2007, pp.176-201.
- [4] C. Sun, Y. Xie, P. Yao, L. Zhang, J. Miles, W. Cook, R. Hui, "Development of ceramic coatings for metallic components in supercritical water-cooled reactors", 2nd Canada-China Joint Workshop on Supercritical-Water-Cooled Reactors, 2010 April 25-28, Paper No.42.
- [5] Peter Kritzer, "Corrosion in high-temperature and supercritical water and aqueous solutions: a review", *Journal of Supercritical Fluids*, Vol.29,2004, pp. 1-29.
- [6] G.S. Was, T.R. Allen, "Time, temperature and dissolved oxygen dependence of oxidation of austenitic and ferritic-martensitic alloys in supercritical water", Proceedings of ICAPP '05, Seoul, Korea, 2005 May, Paper 5690 .
- [7] Q. J. Peng, S. Teyseyre, P. L. Andresen, and G. S. Was, "Stress corrosion crack growth in Type 316 stainless steel in supercritical water", *Corrosion*, Vol. 63, Iss. 11, 2007, pp. 1033-1041.
- [8] S. Teyseyre, Z. Jiao, E. West, and G.S. Was, "Effect of Irradiation on stress corrosion cracking in supercritical water", *Journal of Nuclear Materials*, Vol. 371, Iss. 1-3, 2007, pp.107-117
- [9] S. S. Hwang, B. H. Lee, J. G. Kim and J. Jang, "SCC and corrosion evaluations of the F/M steels for a supercritical water reactor", *Journal of Nuclear Materials*, Vol. 372, 2008, pp. 177-181.
- [10] Y. Yi, B.Lee, S. Kim and J. Jang, "Corrosion and corrosion fatigue behaviors of a 9Cr steel in a supercritical water condition", *Mater. Sci. Eng. A*, Vol. 429, 2005,161-168.
- [11] Yun Chen, Kumar Sridharan, Todd Allen, "Corrosion behavior of ferritic-martensitic steel T91 in supercritical water", *Corrosion Science*, Vol. 48, 2006, pp. 2843-2854.
- [12] P. J. Buongiorno and P. E. MacDonald, "Progress report for the FY-03 Generation-IV R&D activities for the development of the SCWR in the U.S.", INEEL/EXT-03-01210, Sept. 2003.

- [13] Q.J. Peng, S. Teysseyre, P. L. Andresen and G.S. Was, “Stress corrosion crack growth in 316 stainless steel in supercritical water”, *Corrosion*, Vol. 63, Iss. 11, 2007, pp.1033-1041.
- [14] Y. Chen, K. Sridharan. T.R. Allen, “Corrosion of candidate austenitic stainless”, NACE International, Houston, TX, 2005, Paper No. 05391.
- [15] H. Lee, S. Son, K. Hwang and C. Lee, “Surface chemical analysis on the corrosion of alloys in the supercritical water oxidation of halogenated hydrocarbon”, *Industrial and Engineering Chemistry Research*, Vol.45, 2006, pp. 3412-3419.
- [16] S. Teysseyre and G.S. Was, “Stress corrosion cracking of austenitic alloys in supercritical water”, *Corrosion*, Vol. 62, Iss. 12, 2006, pp.1100-1116.
- [17] B. Geddes, X. Huang and D. Guzonas, “Potential use of ceramic materials for supercritical water-cooled reactors”, 2nd Canada-China Joint Workshop on Supercritical-Water-Cooled Reactors, 2010, April 25-28, Paper No.69.
- [18] P. Kritzer, N. Boukis, and E. Dinjus, “Corrosion of alloy 625 in aqueous chloride and oxygen containing solutions”, *Corrosion*, Vol.54, Iss. 10, 1998, Paper No. 98100824.
- [19] M. Nagae, T. Yoshio and K. Oda, “Corrosion behavior of structural ceramics in supercritical water”, 11th International Ceramic Congress, Advances in Science and Technology, Vol. 4, 2006, pp.173-177.
- [20] Kohei Oda and Tetsuo Yoshio, “Hydrothermal corrosion of alumina ceramics”, *Journal of American Ceramic Society*, Vol. 80, Iss. 12, 1997, pp.3233–3236.
- [21] G. Goward, D. Boone and F. Pettit, US Patent No. 3,754,903 (1973)
- [22] P. Sahoo and G. Goward, “Advances in thermal spray science and technology”, Proceedings of the 8th National Thermal Spray Conference, Houston, United States, 1995 Sept. 11-15, pp. 539-544.
- [23] G. Goward, Proceedings of the Symposium on Properties of High Temperature Alloys with Emphasis on Environmental Effects, Vol. 77, Iss. 1, 1976, pp. 806-823.
- [24] R. Hecht, G. Goward and R. Elam, US Patent No. 3,928,026 (1975).
- [25] Atomic Energy of Canada Limited, Canada enters the nuclear age: a technical history of Atomic Energy of Canada Limited, McGill-Queen's Press, 1997.
- [26] A. Ul-Hamid, “A TEM study of the oxide scale development in Ni–Cr–Al alloys”, *Corrosion Science*, Vol. 46, 2004, pp. 27–36.
- [27] Y. Watanabe, K. Shoji, T. Adschiri, K. Sue, “Effects of oxygen concentration on corrosion behaviour of alloys in acidic supercritical water”, Corrosion 2002, NACE International, Houston, TX, Paper No. 2355.
- [28] P. Puetz, X. Huang, and Q. Yang, “Characterization of Transient Oxide Formation on NiCrAlY after Heat Treatment in Air”, submitted to *Surface and Coating Technology*, 2010.